Hydrogen ion passivation of multicrystalline silicon solar cells

J.C. Muller, A. Barhdadi, Y. Ababou, P. Siffert

Revue Phys. Appl. **22** (1987) 649-654 JUILLET **1987**, PAGE 649

Classification
Physics Abstracts
60.30 — 72.40 — 61.70T — 81.60

Hydrogen ion passivation of multicrystalline silicon solar cells

J. C. Muller, A. Barhdadi, Y. Ababou and P. Siffert

CRN (IN2P3), Laboratoire de Physique et Applications des Semiconducteurs (PHASE) (U.A. DU CNRS n° 292), 23, rue du Loess, 67037 Strasbourg Cedex, France

(*Reçu le 26 septembre 1986, accepté le 18 décembre 1986*)

Résumé. — Il est reconnu que l'hydrogène peut être choisi pour passiver les défauts présents dans les matériaux polycristallins. Du point de vue technique, la meilleure approche consiste à utiliser l'implantation d'ions hydrogène à faible énergie (0,5 à 5 keV) avec une source du type Kaufman ou similaire, afin de réduire la durée du traitement. Pour notre source à faisceaux multiples, nous avons déterminé la distribution effective et le profil de concentration de l'hydrogène introduit, les modifications des propriétés optiques et les conditions pour lesquelles deux matériaux multicristallins massifs (POLYX et SILSO) donnent le plus grand gain de rendement de conversion photovoltaïque.

Abstract. — It has been recognized that hydrogen can be chosen to passivate the defects present in polycrystalline materials. Technically, the best approach is to use hydrogen ion implantation at low energy (0.5 to 5 keV) by means of a Kaufman or similar type ion source in order to reduce the processing time. For our multiple beam ion source, we have determined the effective concentration profile of the introduced hydrogen, the modification of the optical properties of the implanted wafers and the conditions under which two multicrystalline materials (POLYX and SILSO) will give the greatest improvement in solar cell performance.

1. Introduction.

Recent investigations have shown that the use of hydrogen ion implantation to passivate grain boundaries and electrically active defects inside the grain might be a way to improve the efficiency of cast and ribbon polycrystalline materials. The ionic procedure for hydrogen treatment has a number of advantages over the conventional plasma method, namely controllable process temperature, shorter duration, and the possibility of operating on cells after metallization of the grid. Thus, the use of a Kaufman type ion source brings this technique close to industrial feasibility [1-7].

In this paper, we propose an alternative method of achieving a high current density for low energy hydrogen implantation by using a multiple beam ion source based on the same principe ás the Kaufman source, but equipped with a post acceleration having an energy range of 0.5 to 5 keV [8-10].

Our goal was first to determine the distribution profile and the concentration of implanted hydrogen by using the inverted nuclear reaction analysis $^{1}H(^{15}N, {}^{4}He\ \gamma)\ ^{12}C$ at an energy of 6.4 MeV and to study the influence of the introduced hydrogen atoms on the doping level and on the top layer of a n^{+}/p junction by using Rutherford Backscattering (RBS), Secondary Ion Mass Spectroscopy (SIMS), ellipsometry and spectrophotometry analyses. Crystallographic and contamination aspects, as well as changes in the optical properties, were also investigated.

Dark properties of the n^{+}/p diffused junction before and after hydrogenation were studied in order to determine the influence of the incident ions on the different components of the dark current and on the sheet resistance. These data were correlated with Light Beam Induced Current (LBIC), spectral response and Deep Level Transient Spectroscopy (DLTS) measurements to detect the presence of electrically active defects in the surface region.

Finally, we have performed a systematic study of the implantation parameters [10-13] to find the conditions (dose, energy, temperature) under which hydrogen ion bombardment of two cast multicrystalline materials (POLYX grown by CGE and SILSO from WACKER) yields optimal solar cell performance.

2. Experimental procedure.

2.1 SAMPLES. — The crystallographic analyses were performed on ⟨111⟩ oriented p-type monocrystalline silicon wafers and the electrical measurements on monocrystalline n^+/p junctions having the same resistivity (about 1 Ω.cm) as materials used in photovoltaic applications. The object of these measurements was to determine the electrical and optical effects of the hydrogen ion bombardment before carrying out a systematic investigation of cell parameters for the two multicrystalline materials.

2.2 HYDROGENATION. — The hydrogenation was performed just before the analysis by implantation of hydrogen ions extracted from the multiple beam ion source whose schematic diagram is shown in figure 1. This source has two molybdenum extraction electrodes perforated with more than 300 holes to give an uniform beam over an 80 cm^2 area. The source is equipped with a post acceleration allowing implantation energies between 0.5 and 5 keV. A total current of 50 mA, corrected for secondary electron emission, can be obtained at 1 keV. This leads to a beam flux of 0.6 mA/cm^2, an incident power (irradiance) of 50 W and consequently to significant target heating (more than 400 °C for an isolated sample holder at equilibrium).

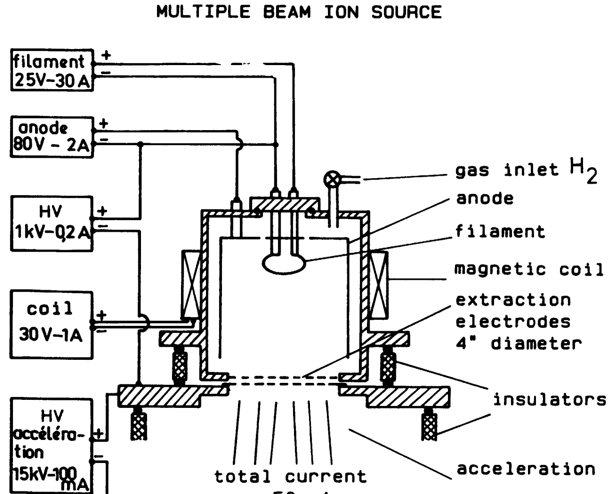

Fig. 1. — Multiple beam ion source, similar to a Kaufman structure, but equipped with a post-acceleration.

3. Macroscopic analysis.

3.1 DISTRIBUTION OF HYDROGEN IONS. — One of the resonance energies at 6.4 MeV of the $^1H(^{15}N, ^4He\ \gamma)\ ^{12}C$ reaction was used for measuring the hydrogen depth distribution as shown on figure 2 for hydrogen ions accelerated to 2 keV and for

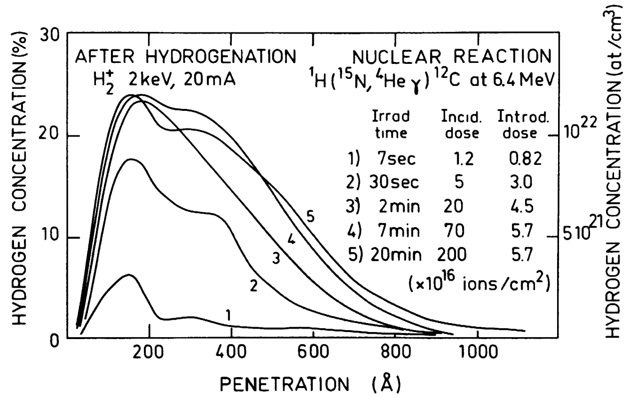

Fig. 2. — Hydrogen distribution obtained by the $^1H(^{15}N, ^4He\ \gamma)\ ^{12}C$ nuclear reaction at 6.4 MeV. Profiles were obtained after deducing the surface peak for different hydrogen implantation times.

different irradiation times. We observed, after deducing the surface hydrogen contamination peak, that the maximum concentration reaches 10^{22} atoms/cm^3 and that a saturation effect occurs for the introduced dose. We also found two distinct peaks, attributed to hydrogen ions having 1 and 2 keV energies respectively. The first value is due to the splitting of the molecular ion into two atoms each having 50 % of the total energy. If we take into account the sputtering of the surface, the energies deduced from each component are in good agreement with theoretical values [10].

3.2 CONTAMINATION. — SIMS measurements have been performed in order to detect the impurities accompanying the beam. The main impurities detected tungsten and molybdenum most probably come from the filament and the extraction grids. The other impurities chromium and copper probably come from the target holder, with the carbon arises from the pumping system [10].

3.3 CRYSTALLOGRAPHIC MODIFICATIONS. — RBS measurements have shown [14, 15] that the first effect of hydrogen ions is to amorphize the material over a thickness of about 500 Å, if the corrected beam flux is set at about 0.12 mA/cm^2 for more than 45 s. This surface amorphization is due to the very high concentration of hydrogen ions and also to impurities like tungsten and molybdenum.

3.4 CHANGES IN OPTICAL PROPERTIES.

3.4.1 *Reflectivity measurements.* — In figure 3 we show typical UV reflectance measurements in the wavelength range 250-800 nm for a silicon sample irradiated with hydrogen ions. One sees that the peak at 275 nm has completely disappeared confirming that we have reached the amorphization level. The second peak at 365 nm is broader and the reflectivity values over the whole visible region are

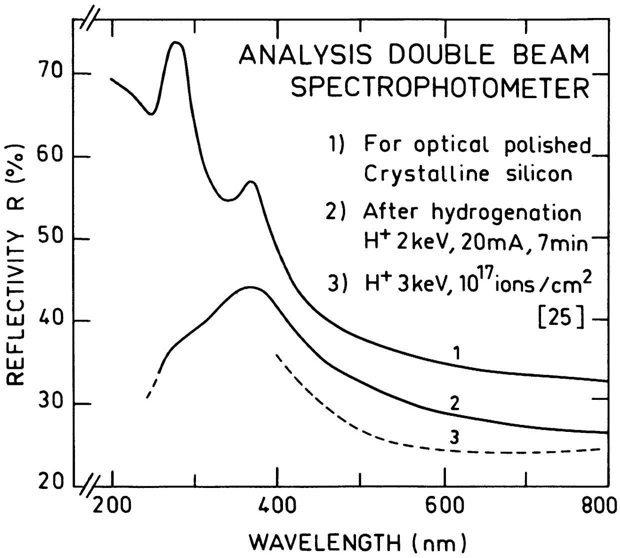

Fig. 3. — Reflectivity measurements as obtained with a Beckmann double beam spectrophotometer before and after hydrogen ion implantation.

lowered by about 5 % as values reported by Sharp *et al.* [16].

3.4.2 *Ellipsometry measurements.* — The absorption coefficient measured at a wavelength of 633 nm shows an increase in the absorption coefficient from the typical value reported for an optically polished sample to a value close to that reported for amorphous silicon [10].

In view of these results, one concludes that short wavelength photons will be absorbed closer to the surface in a region in which the diffusion length is lower, so that a decrease in internal quantum efficiency in this region can be expected, whereas the absorption of the near infrared photons (0.9-1.1 μm) will be enhanced.

4. Electrical effects on monocrystalline silicon.

4.1 Virgin samples. — The measurements were performed on Schottky diodes. After hydrogen implantation, the *C-V* characteristics show anomalous effects near the surface at voltages values below 1 V, up to a depth equivalent to the implanted profile penetration. Normal Schottky diode parameters were subsequently obtained on the same samples after the removal of a 400 Å thick layer by anodic oxidation [14, 15, 17]. However, DLTS analysis showed the presence of one dominant peak which acts as a compensating centre in P-type material, and which is still present even with the removal of a 1 000 Å thick layer. This defect disappeared after thermal annealing at a temperature lower than 400 °C [14, 15, 17].

We have also shown [18] that the implanted hydrogen ions completely remove the defects created by pulsed laser irradiation in virgin silicon.

3.2 n^+/p junctions. — In a previous paper [17], it was shown that the diffusion part of the direct dark current of a n^+/p junction could be affected by the hydrogen implantation process. This effect, attributed to the creation of the surface recombination centres seen in DLTS, can also be detected by experiments involving highly absorbed light.

LBIC measurements conducted at a wavelength of 0.45 μm over adjacent implanted and unimplanted regions revealed a degradation of the photoresponse in the hydrogen treated region. However, LBIC scans performed at 0.80 μm showed an increased signal.

These two results have been confirmed by measurements of the spectral response of a 2 cm² n^+/p diffused cell (see Fig. 4). The improvement in the infrared region should not be explained by an increase of the diffusion length in the bulk, but rather by a change in the absorption and reflection coefficients in the surface layer as earlier stated.

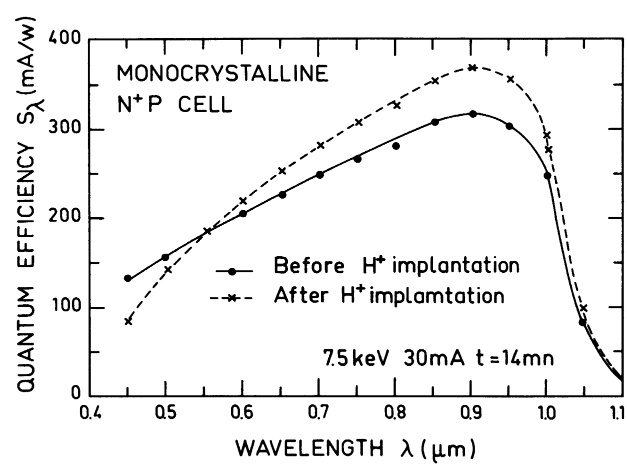

Fig. 4. — Spectral response of a 2 cm² n^+/p diffused monocrystalline cell before and after hydrogen ion implantation.

5. Improvement of the photovoltaic characteristics.

The *I-V* characteristics have been measured on both POLYX and SILSO samples having resistivities between 1 and 2 Ω.cm. For the former material, slices were taken from the top, middle and bottom of the ingot. Small classical diffused cells of 2 cm² area were supplied by Telefunken and the Compagnie Générale d'Electricité (CGE). The hydrogen implantation was performed on the metallized cells.

5.1 Sheet resistance measurements. — After hydrogenation, we observed a systematic increase of the sheet resistance values. This can be better explained by the fact that the active dopant distribution is modified by hydrogen-associated defects which reduce the carrier mobility in this highly doped n^+ layer as we have previously reported for an implanted ^{75}As layer initially activated using laser annealing and partially deactivated after hydrogen bombardment [10]. The decrease of the number of active dopants after hydrogen treatment reported by many authors, like Pankove [19] for p type silicon, and only by Johnson [20] for low doped n type can not explain the observed increase in sheet resistance.

5.2 OPTIMIZATION OF THE HYDROGEN IMPLANTATION PARAMETERS. — The implantation parameters dose and energy of the introduced hydrogen ions, are connected to the beam flux and to the incident power which strongly affect the temperature rise of the sample during processing.

By conducting a separate study of some implantation parameters (dose, energy [10, 12, 21]) and temperature (which is yet to be completely optimized), we have found that the greatest improvements in *I-V* characteristics are obtained under conditions of incident power around 0.3 W cm^{-2} and implantation flux/energy combinations in the range 0.1 mA cm^{-2}/3 keV to 0.3 mA cm^{-2}/1 keV respectively, with the sample temperature kept at about 300 °C.

5.3 SOME TYPICAL RESULTS. — The results obtained on POLYX and SILSO cells are given in table I. It can be seen that the improvement in open-circuit voltage V_{oc}, short circuit current I_{sc} and in the efficiency is greater when these initial values are lower. The improvement can be significant if the sample temperature is raised to about 300 °C.

In figure 5, we have illustrated this for cells processed on SILSO material, by plotting the evolution of the ΔV_{oc} data as a function of the initial open-circuit value. We conclude that for cells having a V_{oc} value greater than about 585 mV, the passivation will be inefficient.

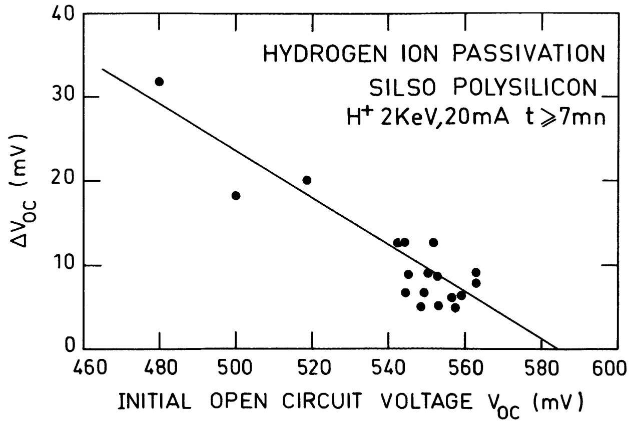

Fig. 5. — Evolution of the enhanced ΔV_{oc} values *vs.* the initial open-circuit voltage as obtained on SILSO materials.

Table I. — *I-V characteristics under illumination of thermal diffused* POLYX *and* SILSO *solar cells, before* (B) *and after* (A) *hydrogen implantation performed with the multiple beam ion source under optimal conditions. Cells were tested on a sun simulator adjusted to deliver* 100 mW/cm^2 (AM1 *conditions*) *without taking into account the surface covered by the grid* ($\simeq$ 10 %). *The results are given for uncoated cells.*

Material		V_{oc} (mV) B	V_{oc} (mV) A	I_{sc} (mA/cm^2) B	I_{sc} (mA/cm^2) A	Fill Factor B	Fill Factor A	η (%) B	η (%) A	$\Delta\eta$ (%)	Temperature
SILSO		546	566	20.7	23.0	0.74	0.71	8.4	9.3	0.9	uncontrolled T < 300°C
		551	565	21.5	23.5	0.74	0.74	8.9	9.8	0.9	
		544	558	19.6	20.5	0.68	0.68	7.3	7.8	0.5	
		543	557	20.7	22.1	0.75	0.74	8.5	9.1	0.6	
POLYX slice from the ingot	middle	545	553	21.1	22.5	0.63	0.62	7.3	7.8	0.5	
		552	552	22.9	24.1	0.73	0.71	9.3	9.5	0.2	
	bottom	541	529	22.8	27.0	0.73	0.69	9.0	9.9	0.9	
		543	532	23.3	26.4	0.75	0.72	9.6	10.5	0.9	
SILSO		541	555	18.7	21.2	0.73	0.74	7.4	8.8	1.4	controlled 300°C
		540	558	19.0	21.5	0.72	0.73	7.4	8.9	1.5	
		541	553	18.5	20.7	0.74	0.74	7.6	8.6	1.0	
		541	561	19.3	21.9	0.73	0.69	7.6	8.6	1.0	controlled 400°C
		543	562	19.4	22.0	0.74	0.70	7.8	8.7	0.9	
		539	559	19.3	21.9	0.73	0.70	7.5	8.6	1.1	

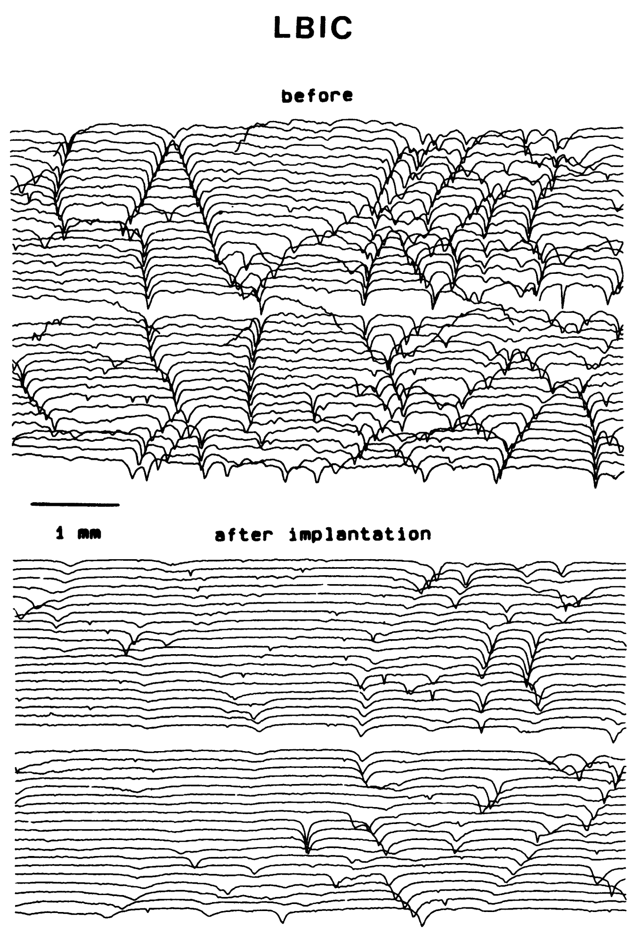

Fig. 6. — LBIC analysis conducted at a wavelength of 0.80 μm on a SILSO cell before and after hydrogen implantation (1 keV, 20 mA, 7 min, temperature $\simeq$ 300 °C).

5.3.1 *Effects of hydrogen ions on the grain boundaries.* — The LBIC analyses were generally performed at a wavelength of 0.80 μm. The most important effect observed in a previous study (see Fig. 20 of Ref. [10]) is an increase in the mean value of the photoresponse, whereas the modification of the contrast of grain boundaries (as reported in Fig. 6 in an arbitrary scale for the current intensity) seems to be a secondary effect with a little contribution to the increase of the I_{sc} value.

5.3.2 *Stability of the process.* — Thermal annealing at 500 °C of some of the hydrogen implanted samples showed that I_{sc} and the LBIC contrast of the grain boundaries returned to their initial values after a two hour processing. At room temperature, all parameters were found to be stable over a long period [22].

6. Conclusion.

We have found that hydrogen ion implantation performed using a multiple beam ion source can be used for passivation of the defects present within the grains as well as at the grain boundaries of multicrystalline materials.

It appears from RBS measurements that the hydrogen distribution follows theoretical range predictions and that the high concentration of hydrogen amorphizes the first 500 Å of the silicon wafer. DLTS analysis shows the presence of a recombination centre in the damaged layer which degrades the photoresponse in the UV region. However, these defects remain less important than the positive aspects gained by the passivation, as is seen by the improvement of the *I-V* characteristics of both cast (POLYX and SILSO) [9, 13] and RAD ribbon solar cells [23] under illumination.

Acknowledgments.

This work was funded by the AFME (Agence Française pour la Maîtrise de l'Energie) and by the PIRSEM from the Centre National de la Recherche Scientifique.

We would like to thank Dr. K. D. Rasch and Dr. W. Schmidt of Telefunken (Heilbronn, FRG), Dr. J. Fally and the members of the Materials Group of the CGE Marcoussis laboratory (France) for kindly supplying industrial diffused solar cells of special shape.

We would also like to thank members of our laboratory, A. Grob for RBS analysis, R. Stuck for SIMS measurements, J. P. Stoquert and S. Unamuno for nuclear measurements, J. J. Grob for the theoretical calculation, A. Slaoui for reflectance measurements, E. Courcelle and D. Salles for interesting discussions and S. Barthe for preparing the devices.

References

[1] SEAGER, C. H., SHARP, D. J., PANITZ, J. K. G. and AIELLO, R. V., *J. Vac. Sci. Technol.* **20** (1985) 430.

[2] HANOKA, J. I., SEAGER, C. H., SHARP, D. J. and PANITZ, J. K. G., *Appl. Phys. Lett.* **42** (1983) 618.

[3] MAUTREF, M., LACROIX, C., BELOUET, C., FAGES, C., BIOTEAU, B. and ARNOULT, F., *Revue Phys. Appl.* **19** (1984) 333.

[4] COM-NOUGUE, J., KERRAND, E., TESSARI, C., COURCELLE, E., MULLER, J. C. and SIFFERT, P., in Palz W. and Fittipaldi F. (eds), Proc. 5th Commission of the European Communities Conf. on *Photovoltaic Solar Energy,* Athens (Greece), October 17-21, 1983 (Reidel, Dordrecht, NL) 1983, p. 1118.

[5] SINGH, R., FONASH, S. J., ROHATGI, A. and RAI CHOUDHURY, P., in Palz W. and Fittipaldi F. (eds), Proc. 5th Commission of the European Communities Conf. on *Photovoltaic Solar Energy,* Athens (Greece), October 17-21, 1983 (Reidel, Dordrecht, NL), 1983, p. 1064.

[6] JOHNSON, J. E., HANOKA, J. F. and GREGORY, J. A., Proceeding of the 18th IEEE Photovoltaic Spec. Conf., Las Vegas (Nevada) oct. 21-25, 1985, p. 1112.

[7] AMMOR, L. and MARTINUZZI, S., *Solid State Electron.* **29** (1986) 1.

[8] MULLER, J. C. and SIFFERT, P., Int. Messe für Bauelementefertigung, Sept. 1982, Wiesbaden (FRG), Bd. 2, p. 107.

[9] MULLER, J. C., COURCELLE, E., SALLES, D. and SIFFERT, P., *NIM Phys. Res.,* **B 6** (1985) 394.

[10] MULLER, J. C., ABABOU, Y., BARHDADI, A., COURCELLE, E., UNAMUNO, S., SALLES, D., SIFFERT, P. and FALLY, J., *Solar Cells* **17** (1986) 201.

[11] COURCELLE, E., ABABOU, Y., MULLER, J. C., SALLES, D. and SIFFERT, P., Proc. 17th Photovoltaic Specialists Conf., Orlando, FL, 1984 (IEEE, New York), p. 601.

[12] ABABOU, Y., GROB, A., MULLER, J. C., SLAOUI, A., STOQUERT, J. P., STUCK, R., TOULEMONDE, M., ZUNDEL, T. and SIFFERT, P., in Pinard P. and Kalbitzer S. (eds), Proc. of 2nd MRS Europe Conf. Strasbourg (Fr.), June 5-8 (1984) Poly- mono-crystalline and Amorphous Semiconductors (Les Editions de Physique), 1984, p. 121.

[13] MULLER, J. C., ABABOU, Y., BARHDADI, A., MESLI, A., TOULEMONDE, M. and SIFFERT, P., *NIM in Phys. Res.* **7/8** (1985) 304.

[14] BARHDADI, A., PONPON, J. P., GROB, A., GROB, J. J., MESLI, A., MULLER, J. C. and SIFFERT, P., *Vacuum* **36** (1986) 705.

[15] BARHDADI, A., Thesis, Louis Pasteur University, Strasbourg (Fr.), 1985.

[16] SHARP, D. J., PANITZ, J. K. G. and SEAGER, C. H., *Thin Solid Films,* **95** (1982) 369.

[17] BARHDADI, A., MESLI, A., ABABOU, Y., COURCELLE, E., SIFFERT, P., in Pinard P. and Kalbitzer S. (eds), Proc. of 2nd MRS Europe Conf. Strasbourg (Fr.), June 5-8 (1984) *Poly- monocrystalline and Amorphous Semiconductors* (Les Editions de Physique), 1984, p. 373.

[18] SLAOUI, A., BARHDADI, A., MULLER, J. C. and SIFFERT, P., *Appl. Phys.* **A 39** (1986) 3184.

[19] PANKOVE, J. I., CARLSON, D. E., BERKEYHEISER, J. E., WANCE, R. O., *Phys. Rev. Lett.* **51** (1983) 2224.

[20] JOHNSON, N. M., HERRING, C., CHADI, D. J., *Phys. Rev. Lett.* **56** (1986) 769.

[21] ABABOU, Y., Thesis, Louis Pasteur University, Strasbourg (Fr.), 1985.

[22] ZUNDEL, T., AFME Contract report 1985 (unpublished).

[23] COURCELLE, E., MULLER, J. C., SIFFERT, P. and BELOUET, C., *Solar Cells* **14** (1985) 157.